World Academy of Science, Engineering and Technology
International Journal of Mechanical and Mechatronics Engineering
Vol:7, No:3, 2013

Aeroelasticity Analysis of Rotor Blades in the First Two Stages of Axial Compressor in the Case of a Bird Strike

R. Rzadkowski, V. Gnesin, M. Drewczyński, and R. Szczepanik

Abstract**—**A bird strike can cause damage to stationary and rotating aircraft engine parts, especially the engine fan. This paper presents a bird strike simulated by blocking four stator blade passages. It includes the numerical results of the unsteady low-frequency aerodynamic forces and the aeroelastic behaviour caused by a non-symmetric upstream flow affecting the first two rotor blade stages in the axial-compressor of a jet engine. The obtained results show that disturbances in the engine inlet strongly influence the level of unsteady forces acting on the rotor blades. With a partially blocked inlet the whole spectrum of low-frequency harmonics is observed. Such harmonics can lead to rotor blade damage. The low-frequency amplitudes are higher in the first stage rotor blades than in the second stage. In both rotor blades stages flutter appeared as a result of bird strike.

Keywords**—**Flutter, unsteady forces, rotor blades.

I. Introduction

FOREIGN objects entering aircraft engines are a perennial problem. Mathematical analysis and computer simulations can provide information on component stresses already in the design phase.

Foreign objects (e.g. a bird) were characterized as a water-like hydrodynamic response by Wilbeck and Rand [1] in their tests. Storace et al. [2] developed a computer program to predict structural response due to soft body impact. Heidari et al. [3] developed rotor dynamics as a nonlinear transient analysis for a propulsion system during bird strike induced fan blade loss. Experiments were carried out on SO-3 compressor first stage rotor blades [4] to initiate a crack by placing rectangular blocks on the stator blades, simulating birds engulfed in the engine.

The Fluent code was used to analyze the low frequency excitation caused by inlet blockage of 1.5 stages of an SO-3 engine, but it did not take into account rotor blade vibration [5, 6]. Aeroeleastic behavior of rotor blade 1.5 first compressor stage was analyzed by Rzadkowski et al. [7].

In this paper the unsteady forces acting on rotor blades will be calculated for a 3D non-viscous ideal gas flow through 2.5 compressor stages using an in-house code and taking into account rotor blade vibration.

R. Rzadkowski is with the R. Szewalski Institute of Fluid Flow Machinery, Polish Academy of Sciences in Gdansk, Poland, st. Fiszera 14, 80-952 Gdańsk (z3@imp.gda.pl).

V. Gnesin is with the National Academy of Sciences of Ukraine, 2/10 Pozharsky st., Kharkov, 61046 Ukraine, (gnesin@ipmach.kharkov.ua).

M.Drewczyński. is with the R. Szewalski Institute of Fluid Flow Machinery, Polish Academy of Sciences in Gdansk, Poland, st. Fiszera 14, 80-952 Gdańsk (mdrew@imp.gda.pl).

R.Szczepanik is with the Air Force Institute of Technology, Ksiecia Bolesława 6, 01-494 Warszawa, Poland, (ryszard.szczepanik@itwl.pl).

II. Aerodynamic Model

Blade failures in the first stage of SO-3 compressors were reported in the years 1975-1991 [4]. Experiments were carried out on a first stage rotor blade in an SO-3 engine compressor at the Air Force Institute of Technology in Warsaw to initiate a crack by placing rectangular blocks on the stator blades, which in real life could be caused by birds engulfed in the engine (see Fig. 1a).

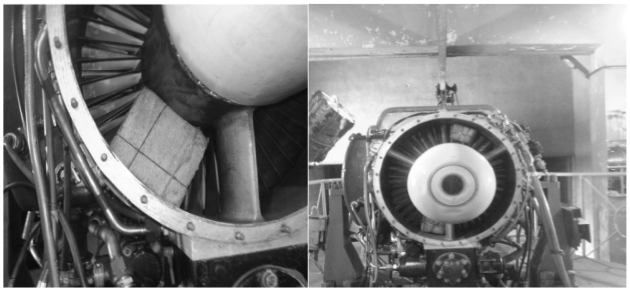

Fig. 1a Test rig of SO-3 engine

The 3D transonic flow of an inviscid non-heat conductive gas through the first compressor stages of an SO-3 aircraft engine was simulated (Fig. 1a).

A 3D whole-annulus model of the first stage of a SO-3 jet engine compressor is shown in Fig. 1b. The model consists of 44 blades in the Inlet Stator Cascade (S0), 28 blades in the Rotor Cascade (R1), 33 blades in the Stator Cascade of the first stage (S1), 42 (R2) rotor blades and 44 (S2) stator blades. The numerical calculations were carried out using computational H-grids: 10*40*84 grid points for the S0 passage, 10*60*78 for the R1 passage, 10*48*68 for the S1 passage, 10*44*64 for the R2 passage and 10*42*62 for the S2 passage. In order to model the engine inlet bird strike, four stator blade passages were blocked.

The spatial transonic flow, including in the general case strong discontinuities in the form of shock waves and wakes behind the exit edges of blades is written in the relative Cartesian coordinate system rotating with constant angular velocity ω according to full non-stationary Euler equations, presented in the form of integral conservation laws of mass, impulse and energy [9].

Each of the passages is discretized, using an H-type grid for the stators domain and a hybrid H-H grid for the rotor domain

([10], [11]). Here the outer H-grid of the rotor remains stationary during the calculation, while the inner H-grid is rebuilt in each iteration by a given algorithm, so that the external points of the inner grid remain unmoved, but the internal points (on the blade surface) move according to the blade motion.

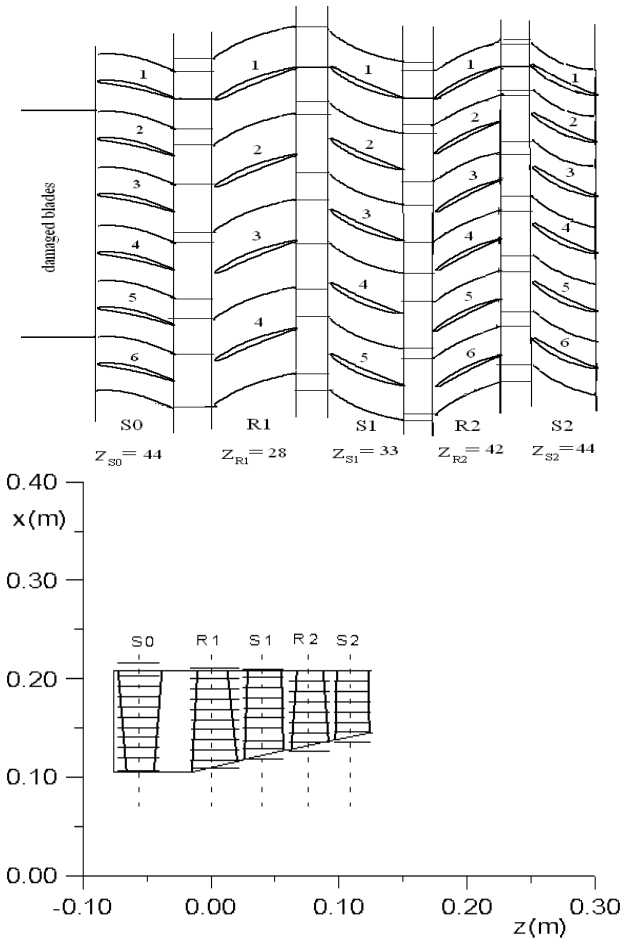

Fig. 1b Computational model of the first stage (S10-R1-S1-R2-S2)

In the general case, when axial velocity is subsonic, at the inlet boundary initial values for total pressure, total temperature and flow angles are used, while at the outlet boundary only the static pressure has to be imposed. Non-reflecting boundary conditions must be used, i.e., incoming waves (three at inlet, one at the outlet) have to be suppressed, which is accomplished by setting their time derivative to zero [8]. On the blade's surface, because the grid moves with the blade, the normal relative velocity is set to zero

$$(v - w)\, n = 0, \tag{1}$$

where v normal velocity vector, w is blade motion vector, n is normal vector.

III. Structural Model

The blade vibration formulation is based on a modal approach of the coupled problem ([11], [12]). The dynamic model of the oscillating blade in linearized formulation is governed by matrix equation:

$$M\,\ddot{u} + C\,\dot{u} + K\,u = F, \tag{2}$$

where *M*, *C*, *K* are the mass, mechanical damping and stiffness matrices of the blade respectively; *u(t)* is the blade displacement; *F* is the unsteady aerodynamic forces vector, which is a function of blade displacement.

The first step of the modal approach consists of solving the problem of the natural mode shapes and eigenvalues without damping and in a vacuum. Then the displacement of each blade can be written as a linear combination of the first *N* modes shapes with the modal coefficients depending on time:

$$u = Uq = \sum_{i=1}^{N} U_i\, q_i \tag{3}$$

where U_i is the displacement vector corresponding to i-th mode shape; $q_i(t)$ is the modal coefficient of i-th mode. Taking into account the equation (3) and the orthogonality property of the mode shapes the equation (2) can be written in form of:

$$I\ddot{q} + H\dot{q} + \Omega q = \lambda(t), \tag{4}$$

where I =diag (1, 1, ... 1), H =diag (2 h_1, 2 h_2 , ... 2 h_n), Ω =diag (ω_1^2, ω_2^2 , ... , ω_n^2) are diagonal matrices; ω_i is i-th natural blade frequency; $\{\lambda(t)\}$ is the modal forces vector corresponding to the mode shapes, $h_i = \omega_i \xi_i$, where ξ_i is the i-th modal damping coefficient ([11]). Thus the dynamic problem (2) reduces to the set of independent differential equations relatively to modal coefficients of natural modes ([9], [10]):

$$\ddot{q}_i + 2h_i\,\dot{q}_i + \omega_i^2\, q_i = \lambda_i. \tag{5}$$

The equations of motion (5) can be solved using any standard integration method.

The modal forces λ_i are calculated at each iteration with the use of the instantaneous pressure field in the following way ([10]):

$$\lambda_i = \frac{\iint_{\sigma} p\overline{U}_i \cdot \overline{n}^{\circ}\, d\sigma}{\iiint_{v} \rho \overline{U}_i^{2}\, dv}. \tag{6}$$

where p is the pressure along the blade surface.

IV. Numerical Results

The numerical calculations presented below were carried out for the two and half stages of the SO-3 engine compressor.

The blade vibration was defined by taking into account the first five natural mode shapes of the rotating R1 and R2 blades. The values of natural frequencies are given in Table I. Mechanical damping was not taken into consideration. Aerodynamical damping was part of the calculation process [10].

TABLE I
NATURAL FREQUENCIES OF THE ROTATING COMPRESSOR ROTOR BLADES R1, R2

Freq.	1	2	3	4	5
Rotor 1	540	1620	2160	3240	4320
Rotor 2	670	2010	2680	4020	6030

The boundary conditions at the inlet and outlet were as follows: the total pressure in absolute system po = 101000 Pa, total temperature in absolute system T_o =288 K.

The calculation included two regimes. In the first regime the calculations of the unsteady flow through the turbine stage were made by first taking into account the rotor rotation without blade vibration. Next the blades vibration began. The time step was constant for all the calculated domains and defined by the stability condition of the difference scheme of the linearized equations system [11].

A Fourier analysis was used for the time-dependant numerical results:

$$F(t) = F_0 + \sum_{i=1}^{\infty} F_{1i} \cos(2\pi\nu i t) + F_{2i} \sin(2\pi\nu i t),$$

where: F(t) is a physical unsteady load; F_o is the averaged value of load; F_{1i}, F_{2i} are the Fourier coefficients; i is the harmonic number; ν is the 1st harmonic frequency. The rotor rotation time was 0.0039 sec and the rotation frequency was 256 Hz.

The averaged values of unsteady aerodynamic loads acting on rotor blades R1, R2 are presented in Tables II, III.

The average values of circumferential forces were highest in the root, whereas the axial forces and moments were highest in the peripheral blade cross-section.

In the case of the blocked inlet, the 4th low-frequency harmonic of circumferential R1 force was the highest in the root cross-section, the 6th harmonic in the 0.55 L cross-section and the 5th harmonic in the 0.96 L cross-section (Fig. 2a).

TABLE II
THE AVERAGED VALUES OF UNSTEADY LOADS ACTING ALONG THE R1 BLADE, BLOCKED INLET, *S0-R1-S1-R2-S2*

L	F_y [N]	F_z[N]	M [Nm]
0.05	-5.131	-1.161	0.0087
0.5	-4.747	-2.414	0.0201
0.95	-4.747	-3.836	0.0231

TABLE III
THE AVERAGED VALUES OF UNSTEADY LOADS ACTING ALONG THE R2 BLADE, BLOCKED INLET, *S0-R1-S1-R2-S2*

L	F_y [N]	F_z[N]	M [Nm]
0.05	-5.771	-0.693	0.0089
0.5	-5.484	-2.388	0.0232
0.95	-3.22	-2.809	0.0317

The 5th low-frequency harmonic of axial unsteady force has the highest value in the root cross-section, the 6th harmonic in the 0.55 L cross-section, and the 5th harmonic in the 0.96 L cross-section (Fig. 2b).

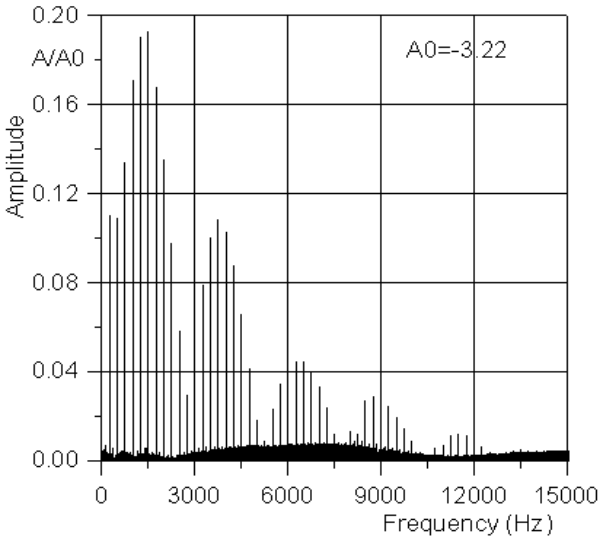

Fig. 2a Amplitude frequency spectrum of circumferential F_y for the peripheral layer of R1 blade

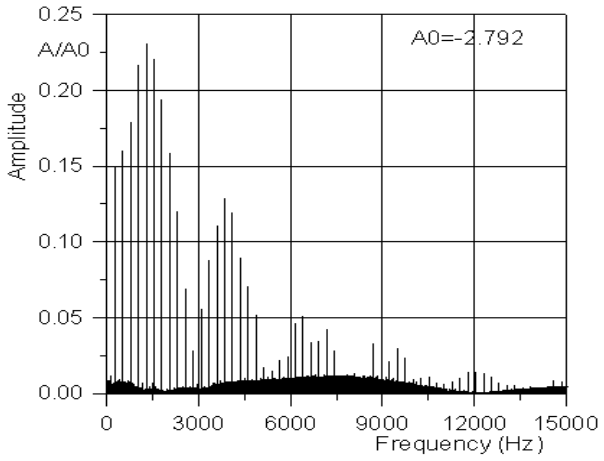

Fig. 2b Amplitude frequency spectrum of axial force F_z for the peripheral layer of R1 blade

The 5th low-frequency harmonic of circumferential R2 force was the highest in the root cross-section, the 5th harmonic in the 0.55 L cross-section, and the 4th harmonic in the 0.96 L cross-section (Fig. 3a).

The 4th low-frequency harmonic of axial R2 force was the highest in the root cross-section, the 4th harmonic in the 0.55 L cross-section, and the 3th harmonic in the 0.96 L cross-section (Fig. 3b).

Therefore the low frequency unsteady force distributions for R1 and R2 blades are different.

The low frequency harmonics of the R2 blade were smaller (10% of steady part) than those of the R1 blades (22%), but the spectrum of frequencies was similar.

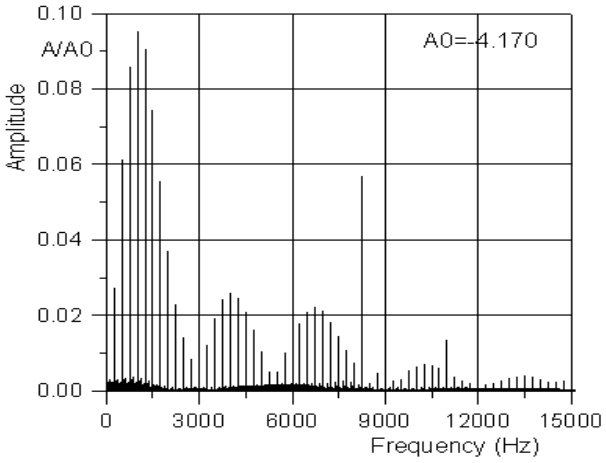

Fig. 3a Amplitude frequency spectrum of circumferential F_y for the peripheral layer of R2 blade

The high-frequency R1 harmonics ($\nu \cdot z_1$=256×33=8448 Hz), 2% of the steady part and ($\nu \cdot z_o$=256×44=11264 Hz) 1%, where ν was the rotation frequency had smaller values than the low-frequency harmonics.

The high-frequency R2 harmonics ($\nu \cdot z$=256×33=8448 Hz) (5%), ($\nu \cdot z_o$=256×44=11264 Hz and ($\nu \cdot z_2$ =256×44 = 11264 Hz)(1%), where ν was the rotation frequency had smaller values than the low-frequency harmonics, but the difference was smaller than in the case of the R1 blades.

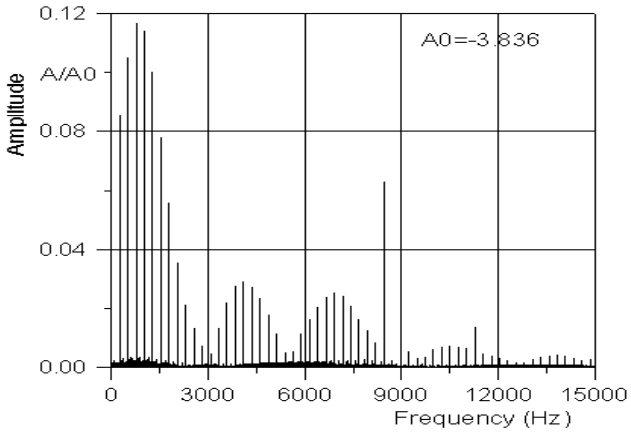

Fig. 3b Amplitude frequency spectrum of axial F_z for the peripheral layer of R2 blade

In the numerical model R1 and R2 rotor blade vibrations were taken into consideration, hence an aeroelastic analysis was possible.

A comparison between the vibration of rotor blades with and without a blocked inlet is discussed below.

The relative harmonic amplitudes of the R1 blade peripheral layer with an unblocked inlet are presented in Table IV. The first natural frequency of R1 blades was 540 Hz (Tab. I), so the frequency in the flow decreased to 500 Hz. The unsteady bending of hy components was 8% of the average displacements. The amplitudes of torsion vibration were 43% of the average twist angle at 500 Hz and 10% at 1500 Hz.

TABLE IV
AMPLITUDE-FREQUENCY SPECTRUM OF GENERALIZED DISPLACEMENTS (HY, HZ, Φ) OF THE PERIPHERAL BLADE LAYER OF THE R1 BLADE, UNBLOCKED INLET, (*S0-R1-S1-R2-S2)*

L	h_y [%] 500 Hz	h_z [%] 500Hz	φ [%] 500 Hz	φ [%] 1500 Hz
0.95	8	9	43	10

The relative harmonic amplitudes of the R1 blade peripheral layer with blocked inlet are presented in Table V. The frequency in the flow is 400 Hz, so it was lower than for the unblock inlet (500Hz). The unsteady bending of hy components was 250% of the average displacements. The amplitudes of torsion vibration were 1000% of the average twist angle at 400 Hz and 2500% at 2500 Hz, so the torsion frequency was also lower than for the unblock inlet (500 Hz).

Therefore blocking the inlet causes a greater decrease of rotor blade vibration frequency in the flow than when the inlet is unblocked. In both cases the form of vibration is bending-torsion and different to the 1st mode shape.

The bending displacement of R1 blades with an unblocked inlet is presented in Fig. 4a. This shows that R1 blades vibrate

with constant amplitude, which means that they are self-excited.

TABLE V
AMPLITUDE-FREQUENCY SPECTRUM OF GENERALIZED DISPLACEMENTS (HY, HZ, Φ) OF THE PERIPHERAL BLADE LAYER OF THE R1 BLADE, BLOCKED INLET, (*S0-R1-S1-R2-S2*)

L	h_y [%] 400 Hz	h_z [%] 400Hz	φ [%] 400 Hz	φ [%] 2500 Hz
0.95	250	230	1000	2500

Fig. 4b shows bending displacement of the R1 blades with a blocked inlet. Here the rotor blade vibration amplitude is considerably higher than in the case of the unblocked inlet, though the blades are also self-excited.

Therefore blocking the inlet causes a greater decrease of rotor blade vibration frequency in the flow than when the inlet is unblocked. In both cases the form of vibration is bending-torsion and different to the 1st mode shape.

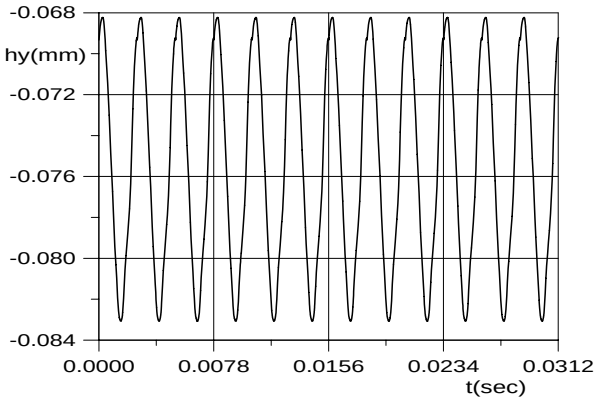

Fig. 4a R1 blade displacement (peripheral layer, axial direction hz), unblocked inlet.

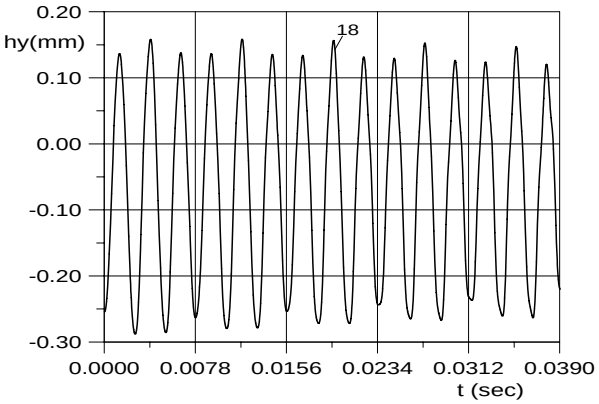

Fig. 4b R1 blade displacement (peripheral layer, axial direction Hz), blocked inlet

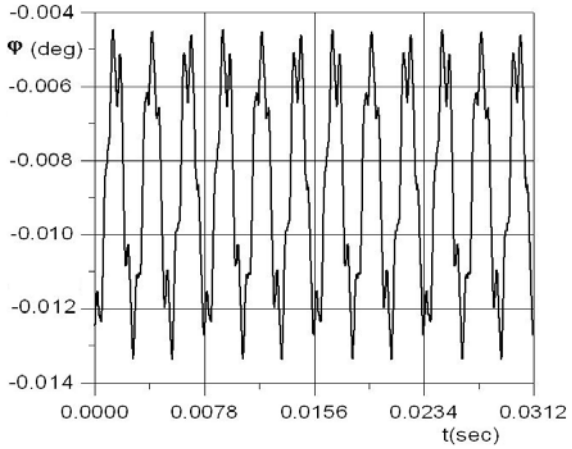

Fig. 4c Amplitude of R1 blade torsional oscillations (peripheral layer), unblocked inlet

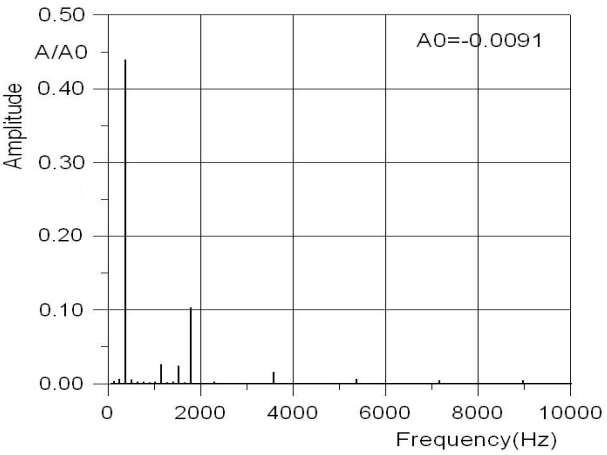

Fig. 4d Frequency spectrum of R1 blade torsional oscillations (peripheral layer), unblocked inlet

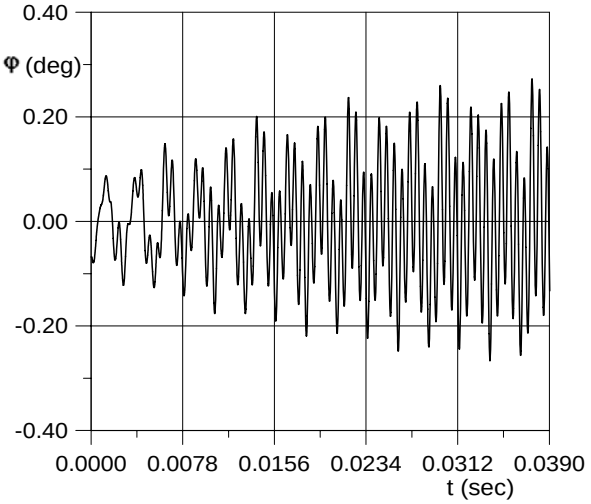

Fig. 4e Amplitude of R1 blade torsional oscillations (peripheral layer), blocked inlet

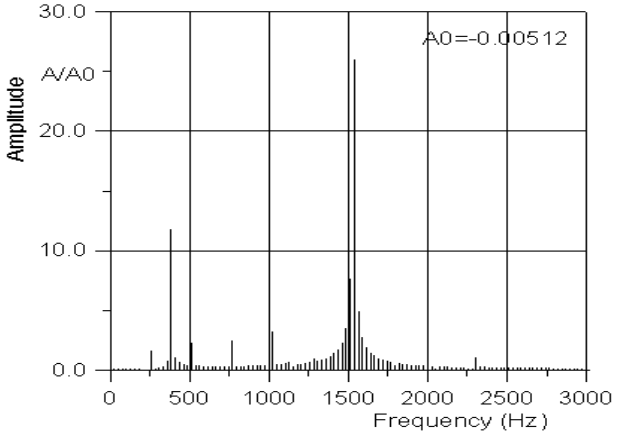

Fig. 4f Frequency spectrum of R1 blade torsional oscillations (peripheral layer), blocked inlet

The torsion angle of R1 blades with an unblocked inlet is presented in Fig. 4c, 4d. This shows that R1 blades vibrate with constant amplitude, which means that they are self-excited.

Fig. 4e, 4f shows the torsion angle of R1 blades with a blocked inlet. Here the rotor blade vibration amplitude is considerably higher than in the case of the unblocked inlet and increases in time. This means that inlet blockage causes flutter.

The relative harmonic amplitudes of the R2 blade peripheral layer with an unblocked inlet are presented in Table VI. The first natural frequency of R2 blades was 670 Hz (Table I), and the frequency in the flow decreased to 500 Hz. The unsteady bending of hy components was 56% of the average displacements. The amplitudes of torsion vibration were 170% of the average twist angle at 500 Hz and 10% at 1500 Hz.

TABLE VI
AMPLITUDE-FREQUENCY SPECTRUM OF GENERALIZED DISPLACEMENTS (HY, HZ, Φ) OF THE PERIPHERAL BLADE LAYER OF THE R2 BLADE, UNBLOCKED INLET, (*S0-R1-S1-R2-S2)*

L	h_y [%] 500 Hz	h_z [%] 500Hz	φ [%] 500 Hz	φ [%] 1500 Hz
0.95	56	52	170	10

TABLE VII
AMPLITUDE-FREQUENCY SPECTRUM OF GENERALIZED DISPLACEMENTS (HY, HZ, Φ) OF THE PERIPHERAL BLADE LAYER OF THE R2 BLADE, BLOCKED INLET, (*S0-R1-S1-R2-S2)*

L	h_y [%] 500 Hz	h_z [%] 500Hz	φ [%] 350 Hz	φ [%] 1800 Hz
0.95	80	80	650	300

R2 blades with an unblocked inlet vibrated with a complex bending –twisting form, bending components at 500 Hz and twisting components at 500 Hz and 1500Hz. This form of vibration is different to the 1st mode shape of the R2 blade.

The relative harmonic amplitudes of the R2 blade peripheral layer with blocked inlet are presented in Table VII. The frequency of bending vibration was 500 Hz, the same as for unblocked inlet, although the unsteady component increased to 80%. The torsion frequency decreased from 500 Hz (unblocked inlet) to 350 Hz and the unsteady part was 650%, i.e. higher than the 170% in the case of the unblocked inlet. The second torsional component frequency increased from 1500 Hz (unblock inlet) (10%) to 1800 Hz (300%).

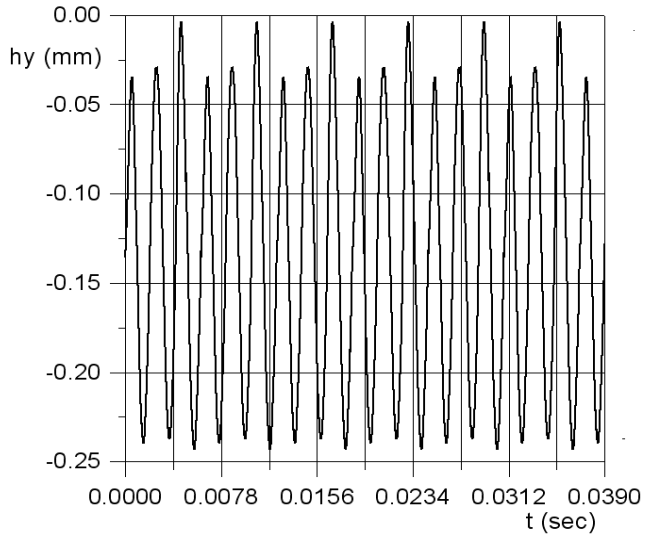

Fig. 5a R2 blade displacement (peripheral layer, axial direction hz), unblocked inlet

Fig. 5a shows bending displacement of R2 blades with an unblocked and Fig. 5b with a blocked inlet. Here the rotor blade vibration amplitude was considerably higher than in the case of the unblocked inlet, though the blades were also self-excited, in the case of the unblock inlet we had damping vibration.

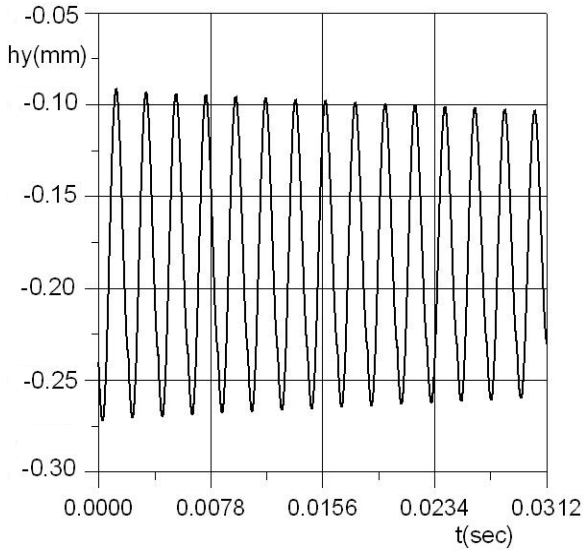

Fig. 5b R2 blade displacement (peripheral layer, axial direction hy), blocked inlet

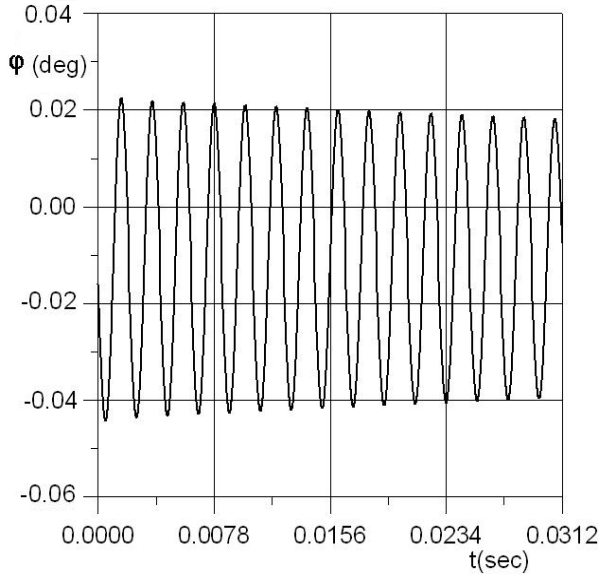

Fig. 5c Amplitude of R2 blade torsional oscillations (peripheral layer), unblocked inlet

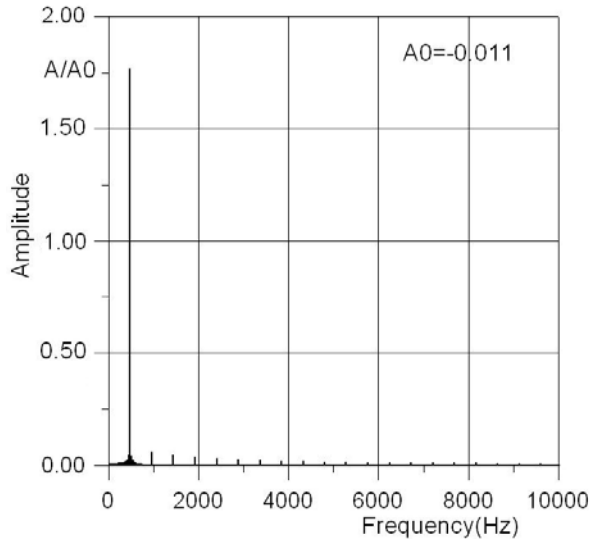

Fig. 5d Frequency spectrum of R2 blade torsional oscillations (peripheral layer), unblocked inlet

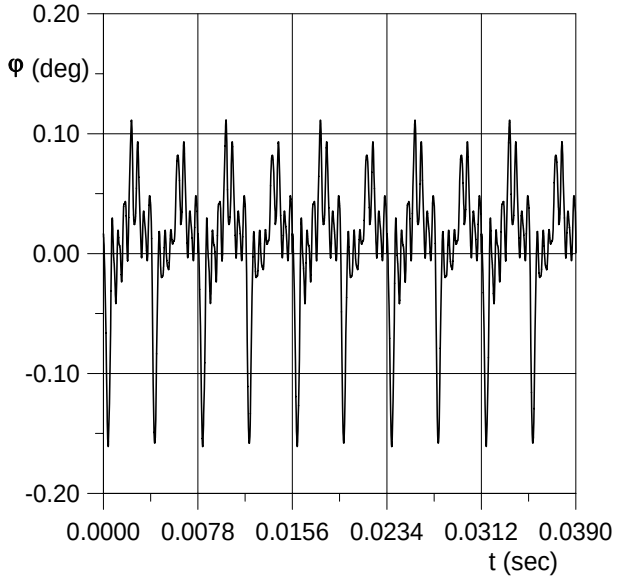

Fig. 5e Amplitude of R2 blade torsional oscillations (peripheral layer), blocked inlet

The torsion angle of R2 blades with an unblocked inlet is presented in Figs. 5c, 5d. This shows that R2 blades have damping vibrations.

Figs. 5e, 5f show the torsion angle of R2 blades with a blocked inlet. Here the rotor blade vibration amplitude was considerably higher than in the case of the unblocked inlet and was self-excited. This means that inlet blockage causes self-excited vibration, but the torsion vibration amplitude did not increase as in the case of the R1 blades.

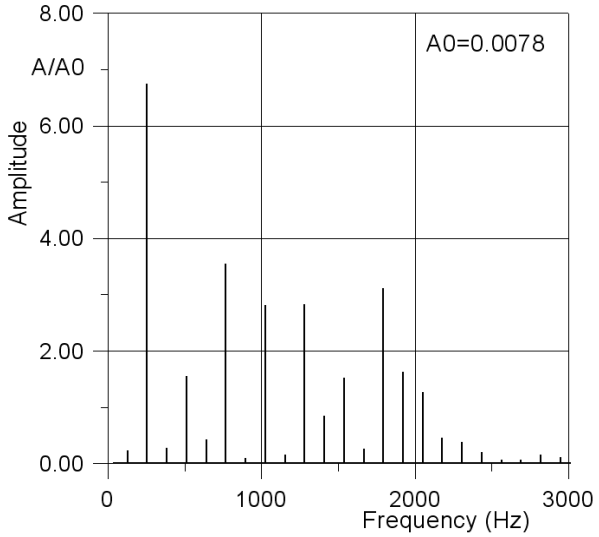

Fig. 5f Frequency spectrum of R2 blade torsional oscillations (peripheral layer), blocked inlet

V. Conclusion

This paper has presented the calculation results for unsteady low-frequency aerodynamic forces acting on SO-3 jet engine compressor R1 and R2 blades, which took into account blade vibration. The forces were analyzed in two

operating conditions: with an unblocked and partially blocked engine inlet. The obtained results show that disturbances in the engine inlet strongly influence the level of unsteady forces acting on the rotor blades. With a partially blocked inlet the whole spectrum of low-frequency harmonics was observed, including the natural frequency of blades.

The vibration amplitudes of rotor blades with a blocked inlet are considerably higher than in the case of an unblocked inlet. Inlet blockage also causes flutter in SO-3 first and second compressor stages. In this case R1 and R2 blade vibrations differ from their first mode shape and include torsional components. The blocked inlet blade vibration mode is different from unblocked inlet blade vibration mode and includes a greater number of torsional components.

ACKNOWLEDGMENT

The authors wish to acknowledge NCBiR for the financial support of this work (project PBS1/B4/5/2012).

All numerical calculations were made at the Academic Computer Centre TASK (Gdansk, Poland).

REFERENCES

[1] J. S. Wilbeck, and J. L. Rand," The Development of a Substitute Bird Model," Journal *of Engineering for Power, ASME*, vol. 103, p. 725, 1981.

[2] A. F. Storace, R. P. Nimmer and R. Ravenhall,"Analytical and Experimental Investigation of Bird Impact on Fan and Compressor Blading, "Journal *of Aircraft,* Vol. 21, July 1984.

[3] M. A. Heidari, D. L. Carlson and T. Yantis, "Rotor-dynamics Analysis Process," *Worldwide Aerospace Conference & Technology Showcase*, April 8 - 10, Toulouse, p 3601, 2002.

[4] R. Szczepanik and R. Rzadkowski, *Dynamic Properties of Aircraft Engine Rotor Blades in Various Operating Conditions*, Biblioteka Problemow Eksploatacji, Radom, (in Polish) 2012.

[5] R. Rządkowski, M. Soliński, and R. Szczepanik, "The Unsteady Low-Frequency Aerodynamic Forces Acting on the Rotor Blade in the First Stage of a Jet Engine Axial Compressor," *Advances in Vibration Engineering*, 11(2), 193-204, 2012.

[6] M. Soliński, R. Rzadkowski, A. Pająk, and R. Szczepanik, "The Unsteady Low-Frequency Forces Acting on the Rotor Blade in the First Stage on an Axial Compressor of SO-3 Jet Engine," *Proceedings of the 8th International Conference on Vibration Engineering and Technology of Machinery*, VETOMAC –VIII, p. 277-278, Gdansk, Sept 3-6, 2012.

[7] R. Rządkowski, V. Gnesin, L. Kolodyazhnaya, and R. Szczepanik, "Aeroelastic Behaviour of First Stage Compressor Rotor Blades with Foreign Object in Engine Inlet," *ISUAAAT'2012, 13TH International Symposium on Unsteady Aerodynamics, Aeroacustics and Aeroelasticity of Turbomachines*, Tokyo, 10-15 Sept, 2012.

[8] S. K. Godunov, *Numerical Solution of Multidimensional Problems in Gasdynamics,* Nauka, Moskva, 1976, (in Russian).

[9] R. Rzadkowski, V. Gnesin, "3D Unsteady Forces of the Transonic Flow Through a Turbine Stage with Vibrating Blades," ASME Paper GT-2002-300311, *ASME TURBOEXPO 2002*, Amsterdam, (June 3-6, 2002) 2002.

[10] V. Gnesin, L. Kolodyazhnaya, R. Rzadkowski, "A Numerical Model of Stator-Rotor Interaction in a Turbine Stage with Oscillating Blades," *Journal of Fluids and Structures*, 19(8), 1141-1153, 2004.

[11] K. Bathe, and E. Wilson, Numerical *Methods in Finite Element Analysis,* Prentice-Hall, Inc Englewood Cliffs, New Jersey, 1976.

[12] R. Rzadkowski, Dynamics *of Steam Turbine Blading, Part Two Bladed Discs,* Ossolineum, Wrocław-Warszawa, 1998.